JMR EARLY CAREER SCHOLARS IN MATERIALS SCIENCE ANNUAL ISSUE: REVIEW

Investigation of thermal transport in composites and ion beam irradiated materials for nuclear energy applications

M. Khafizov,[a] V. Chauhan, Y. Wang, F. Riyad, and N. Hang
Department of Mechanical and Aerospace Engineering, The Ohio State University, Columbus, Ohio 43210, USA
D.H. Hurley
Department of Materials Science and Engineering, Idaho National Laboratory, Idaho Falls, Idaho 83415, USA

(Received 1 July 2016; accepted 24 October 2016)

Thermal transport in materials used for energy applications is a physical process directly tied to performance and reliability. As a result, a great deal of effort has been devoted to understanding thermal transport in materials whose ability to conduct heat is critical. Here, our objective is to discuss the utility of laser-based thermoreflectance (TR) approaches that provide microscale measurement of thermal transport. We provide several examples that implement the TR technique to investigate thermal transport in materials used in nuclear energy applications. First, we discuss utility of this technique to measure thermal conductivity in ion irradiated ceramic materials during investigations where the primary objective is to understand the impact of radiation induced crystalline structure defects on thermal transport. We also present the capability of TR approach to resolve thermal conductivity of each layer in tristructural isotropic fuel, silicon carbide fiber composites, and 2nd phase precipitates in uranium silicide. Finally, the ability to measure interface thermal resistance between adjacent layers in composites is demonstrated.

M. Khafizov

Dr. Marat Khafizov is an assistant professor in the Department of Mechanical and Aerospace Engineering at The Ohio State University (OSU). He obtained his Ph.D. degree in Physics from University of Rochester in 2008. Prior to joining OSU, he was a research scientist at Idaho National Laboratory (INL) from 2010 to 2014. At INL, he performed research aimed at understanding the impact of radiation damage on thermal transport in ceramic materials and was involved with development of laser based methods for characterization of material's physical properties. Dr. Khafizov has an extensive experience in utilizing optical pump probe spectroscopy to study processes important for efficient energy utilization and information processing. He has applied this technique to study dynamics of excitons in carbon nanotubes, electron-hole recombination in semiconductors, superconducting state recovery, propagation of ultrasonic waves and phonon mediated thermal transport. His research findings have contributed to various technological applications including photovoltaics, information processing, radiation detection and nuclear energy. Currently, he is a director of Thermal Properties of Materials for Extreme Environments laboratory.

I. INTRODUCTION

Safe and economic utilization of nuclear energy relies on accurate temperature control of various components within the reactor. A number of physical processes including rates of nuclear reactions, diffusion of fission products, and heat transfer are functions of temperature.[1] Within a solid material, the temperature distribution depends on the ability of a material to conduct heat. Thermal conductivity is the physical property that is used to describe heat transport at the engineering scale level.[2] The objective of this paper is to summarize our studies aimed at understanding the mechanisms of thermal transport in ceramic materials used for nuclear energy applications. We present several examples that utilize a laser-based approach to measure thermal transport in nuclear fuels and related materials.

The primary function of nuclear fuel in fission reactors is to provide fissile atoms that upon absorption of a neutron generate energy.[1] The thermal energy liberated after the fission process must be transferred to the coolant and eventually transformed into electricity using turbines.[3] At the same time, fuel is expected to retain highly radioactive fission products. The latter constitute a primary environmental hazard if released to the surrounding area. The fuel must also maintain its structural integrity.

Contributing Editor: Terry M. Tritt
[a]Address all correspondence to this author.
e-mail: khafizov.1@osu.edu
DOI: 10.1557/jmr.2016.421

Meeting all of these requirements is difficult considering the dramatic structural and chemical changes taking place within the fuel.[4,5]

Efficient utilization of nuclear energy in fission reactors relies on detailed understanding of the fuel behavior under reactor conditions. Fuel performance codes are developed to describe fuel behavior. In these codes, evaluating the temperature distribution within a fuel constitutes a critical step that impacts other predicted performance characteristics. The temperature profile, determined in large part by the thermal conductivity, strongly influences the mechanisms that control structure evolution and fission product behavior.[6–8] This article focuses on how thermal properties of nuclear materials are influenced by their microstructure and its evolution under irradiation.

The discussion presented in this article is structured as follows: In Sec. II, we describe a thermoreflectance (TR) approach used for measurement of thermal conductivity in applications where micron level resolution is required. In Sec. III, we describe the application of TR to investigations of the irradiation effects on thermal conductivity, where ion beam irradiation is used to introduce a thin damage layer at the surface of the material. The damage layer is treated as a thin film having thermal properties that are different from the un-irradiated bulk. In Sec. IV, we discuss the application of the TR techniques to understand thermal transport in composite materials, where heterogeneity must be considered. Each example is accompanied by a discussion illustrating the importance of understanding thermal transport.

II. MEASUREMENT OF THERMAL TRANSPORT

A. Standard approaches for thermal conductivity measurements

Direct measurement of thermal conductivity is achieved by applying a heat flux across a material of a known geometrical shape and measuring the temperature difference across a fixed distance using thermocouples.[9] In general, this approach requires centimeter size samples. While this is in principle a straightforward measurement, a number of other factors need to be accounted for including radiative heat dissipation through the surface of the material as well as thermal interface resistance between thermocouple and material. For high-temperature measurements, large radiative losses through the surface and unavailability of high-temperature thermocouples make direct measurement impractical.[10]

Xenon thermal flash and more recently laser flash method have become the primary methods used for measurement of thermal transport in materials utilized for nuclear applications.[5,11,12] It is applied on a disk shaped specimen with flat parallel surfaces. One side is excited by a short laser pulse and the infrared emission is measured on the other side. The time it takes for the opposite side to be heated is used to quantify the ability of material to conduct heat. Being a transient measurement, laser flash provides measurement of thermal diffusivity. To obtain thermal conductivity one needs to perform an alternative measurement of specific heat and density. In principle, it is possible to calibrate this measurement to measure specific heat as well.[13] This approach is well suited for high-temperature measurements as long as appropriately sized samples are available. The absence of electrical connections makes laser flash attractive for implementation on neutron irradiated samples.

Both techniques described so far are considered as bulk measurements that provide an averaged value across the thickness of the specimen. Many advanced fuel concepts rely on composite materials.[14–16] While for many design and safety analyses the averaged value of thermal conductivity is sufficient, some analyses require spatially resolved measurement of conductivity. This applies to conditions where the exact temperature distribution is critical or where one is tasked with development and validation of model with predictive capability.[8,17,18] The latter typically involves the ability to predict thermal conductivity as a function of radiation induced microstructure.[19] Another limitation of both techniques is their lack of sensitivity to a thin damage layer resulting from ion beam irradiations, which is an alternative method used to simulate displacement damage caused by energetic neutrons and fission products.[20] The ability to perform thermal transport measurement on ion irradiated samples opens up cost attractive possibilities for fundamental studies on the impact of radiation on thermal properties.[21–24]

B. Modulated TR approaches

In the modulated TR approach, two beams are incident on the flat surface of a sample.[25] One beam is used as a heater whose intensity is modulated by a sine or square wave function. The second beam is used as a sensor, whose reflectivity change is used as an indication of temperature changes. TR methods require a polished surface and deposition of a thin metallic transducer layer. This metal transducer layer ensures strong optical absorption of the pump beam and acts as temperature sensor. Small changes in the temperature of the metal layer results in a small reflectivity change. This process is referred to as TR and thus the name for this approach. This TR coefficient is material dependent and also depends on optical wave length.[26] As a result, the metal layer is chosen according to the wave length of the laser.

Various implementations of TR techniques exist. Time domain TR (TDTR) recently has gained popularity in thermal transport studies of thin films. It utilizes an ultrashort pulse to excite a thermal pulse and a probe beam is used to trace the evolution of the temperature on a nanosecond time scale.[27–29] Typically, this technique is

only sensitive to thermal transport in the depth direction.[30] Frequency domain TR (FDTR) uses continuous wave lasers and examines the phase lag between excitation pulse and temperature as a function of a modulation frequency.[31,32]

In this work, we primarily use a variation of TR that relies on spatially resolved measurement where the temperature profile around the excitation spot is measured.[33–35] Our choice of this approach stems from its attractiveness for use in hot cell applications, where the exact knowledge of some of the experimental parameters is not required. Those include spot size of both beams, thickness of the metallic transducer layer, and thermal interface resistance between transducer and material.[31,36] Most of the results presented in the following sections were acquired using a spatial scan TR presented below. We also provide one example where TDTR and FDTR are used.

C. Experimental setup

A schematic representation of spatial domain TR (SDTR) approach is depicted in Fig. 1.[36] The pump and probe beams are derived from two continuous wave diode lasers emitting at 660 nm and 532 nm wave length, respectively. Amplitude modulation of the pump is achieved by direct modulation of the laser output via electronic trigger. Both pump and probe are focused on the sample using a single 50× microscope objective resulting in a spot size of ~1 μm for both beams. Lateral scanning is achieved through an optical two-lens lever.[37] Small changes in reflectivity of the probe beam $\Delta R/R$ ranging from 10^{-5} to 10^{-3} are measured using lock-in amplification of the photodiode voltage signal. We also present a few examples that use a modified version of this setup. The differences will be addressed during the discussion of specific examples.

This arrangement allows a tightly focused, amplitude modulated pump beam to excite a thermal wave inside the material. The frequency of the pump is tuned to confine the thermal wave to either a damage region created by ion irradiation or to a micron sized area on the surface of a heterogeneous sample.[38] Spatially resolved amplitude and phase profiles of the thermal wave are measured by recording reflectivity changes of the probe beam while the pump is laterally scanned on the surface of the sample. The reflectivity change is directly proportional to the change in the surface temperature.

Typical wave profiles obtained from uranium silicide (U_3Si_2) are depicted in Fig. 1(b).[39] The amplitude profile is sharply peaked around the pump and drops off with an exponential-like decay away from the pump. The phase lag is linear with distance when sufficiently away from

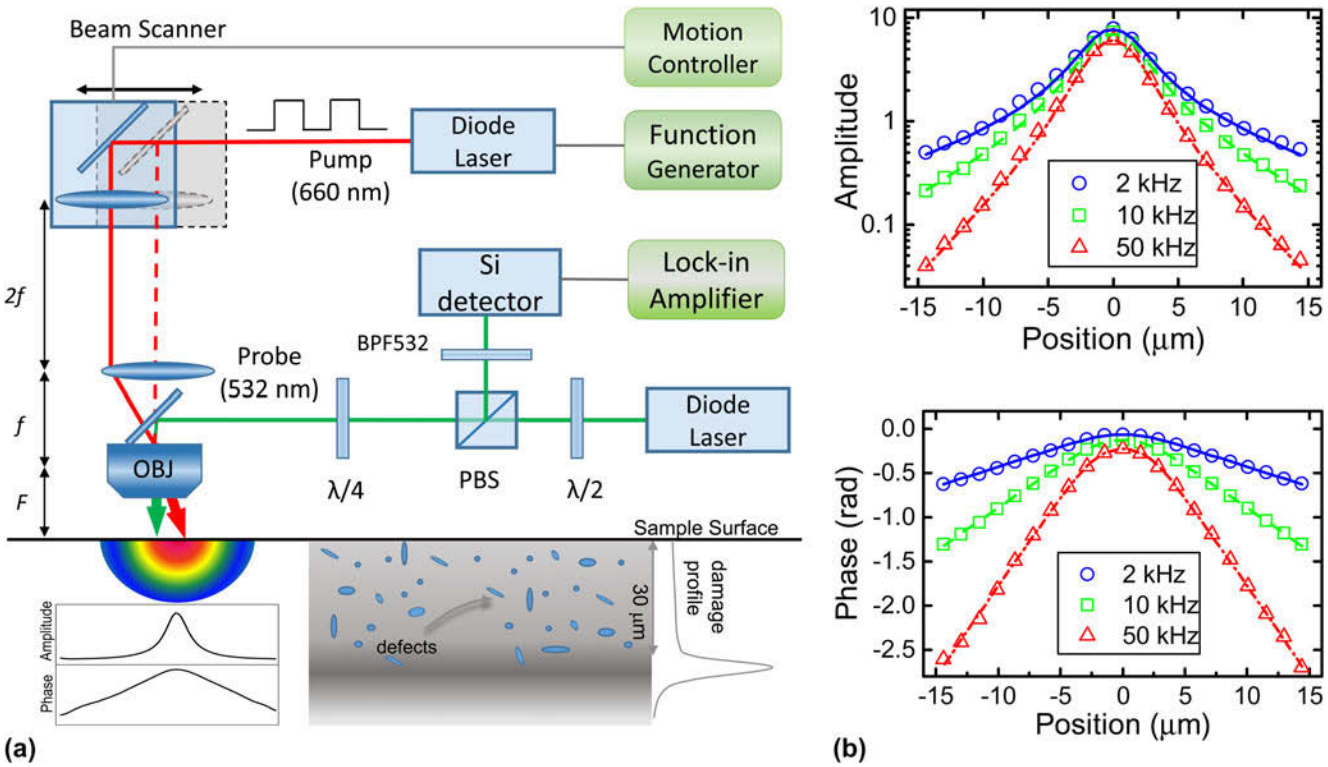

FIG. 1. (a) Experimental layout of SDTR approach. Pump's intensity is harmonically oscillating and is scanned on surface using a two-lens lever system. Probe is fixed and its reflectivity change is recorded. (b) Spatially resolved thermal wave profiles measured on the surface of U_3Si_2 fuel. Both amplitude (top) and phase (bottom) of the wave profile are plotted as a function of pump position along a straight line with probe at the origin. Profiles measured at different modulation frequencies are shown.

the pump. Physically the slope in this region is related to a time required for the heat wave to diffuse a specific distance. This suggests that for a specific modulation frequency the phase lag is larger for materials with lower conductivity.

Measured thermal wave profiles were analyzed using an exact analytical solution of the heat diffusion equation in a two layer system representing thin metal transducer film on top of a substrate that is assumed to be infinitely thick.[33] This assumption is justified when one considers that the thickness of specimens is at least 500 μm and penetration depth of thermal waves considered in our studies is limited to 100 μm for the lowest modulation frequency. The limitations of this assumption when applied to the composites and ion irradiated samples will be addressed further when their examples are discussed. Determination of thermal conductivity for the unknown layer involves fitting of the experimental and model profiles using a least square minimization.[33,36] Using this approach our measured thermal conductivity for U_3Si_2 at room temperature is 7.1 W/m K.

III. MEASUREMENTS IN ION IRRADIATED MATERIALS

In this section, we discuss the utility of TR approaches to the study of thermal transport in ion beam irradiated samples. We discuss several examples where we investigate the impact of irradiation induced point defects, dislocation loops, and fission products on thermal conductivity in fuel surrogates. We first discuss a study aimed at studying the impact of irradiation induced point defects on thermal conductivity of UO_2.[23] In the second example, we investigate the influence of dislocation loops on thermal conductivity in cerium dioxide (CeO_2).[40] Lastly, the impact of fission product on thermal conductivity of fuel is represented by a study of krypton (Kr) ion irradiated silicon carbide.[41]

In addition to the spatially resolving capability of TR techniques one needs to develop carefully tailored ion irradiations. Our irradiation conditions were chosen so that specific defects are generated. For point defects low temperature hydrogen ion (H^+) irradiations were performed.[42] Dislocation loops were fabricated by high-temperature irradiation with H^+ ions.[40] Fission product was introduced by implantation of Kr.[41] While these irradiation conditions do not necessarily reflect the reactor conditions, they were tailored to capture relevant physical mechanisms important for validation of thermal transport models.[43,44] It should be noted that the original intention was to study all of these conditions in UO_2, but has not yet been accomplished due to difficulties that was encountered in performing ion irradiations on UO_2 over a broad range of temperatures and ion fluences that produced samples suitable for TR measurements.

The discussion on the impact of microstructure induced by a fission environment will not be complete without addressing the impact of fission gas bubbles on thermal conductivity. These latter phenomena have been actively investigated by computational methods[19,45,46] and very little experimental data exist and are a subject of future work.[47,48]

The stopping and range of ions in matter (SRIM) code was used to estimate the displacement damage.[49] Calculations were done using the Kinchin–Pease method and the Norgett, Robinson, and Torrens (NRT) model. Estimated damage profiles were approximated by two layers in case of H^+ ions and a single layer in case of Kr ions that have uniform damage to simplify our thermal conductivity analysis. During thermal transport measurement, the modulation frequency of the pump was chosen so that the excited thermal waves were primarily confined to the damaged layer.

A. Thermal conductivity reduction due to point defects

Polycrystalline UO_2 samples fabricated at Los Alamos National Laboratory[50] were irradiated using 2.6 MeV H^+ ions derived from NEC Pelletron Tandem accelerator at the University of Wisconsin.[42] Three samples were irradiated to an estimated fluence of 1.4×10^{17}, 7.0×10^{17}, and 1.4×10^{18} ions/cm^2. The damage profile was calculated using SRIM code with threshold displacement of 40 eV and 20 eV for uranium and oxygen, respectively.[42] It is approximated by two regions, namely the plateau and peak damage regions. In the plateau region, displacement damage is approximately uniform and extends over 32 μm. It is followed by a peak damage region confined to a narrow zone that spans about 4 μm, where most of the damage takes places and majority of hydrogen atoms are implanted. The estimated damage within the plateau regions of all irradiated samples is 0.01, 0.05, and 0.10 displacements per atom (dpa), respectively. Concentration of implanted H atoms within plateau region is less than 0.01 at.%.[42] A thin gold layer of about 50 nm in thickness was thermally evaporated on each sample that acted as the transducer layer for TR measurement.

Typical thermal wave profiles recorded from as-prepared and irradiated UO_2 samples using SDTR are shown in Fig. 2(a). It is noticeable that the slope for the irradiated samples is larger than that of the reference sample. This is a direct indication of reduced thermal conductivity in the irradiated sample. A thermal diffusion model accounting for thermal transport across the damage profile was implemented and a fitting procedure was applied to extract the thermal conductivity of the plateau damage region.[23] In this case, thin metal film, plateau damage layer, peak damage layer, and undamaged substrate are explicitly considered in the heat diffusion model. The results of SRIM were used to determine the thickness of plateau and peak damage layers and their conductivities

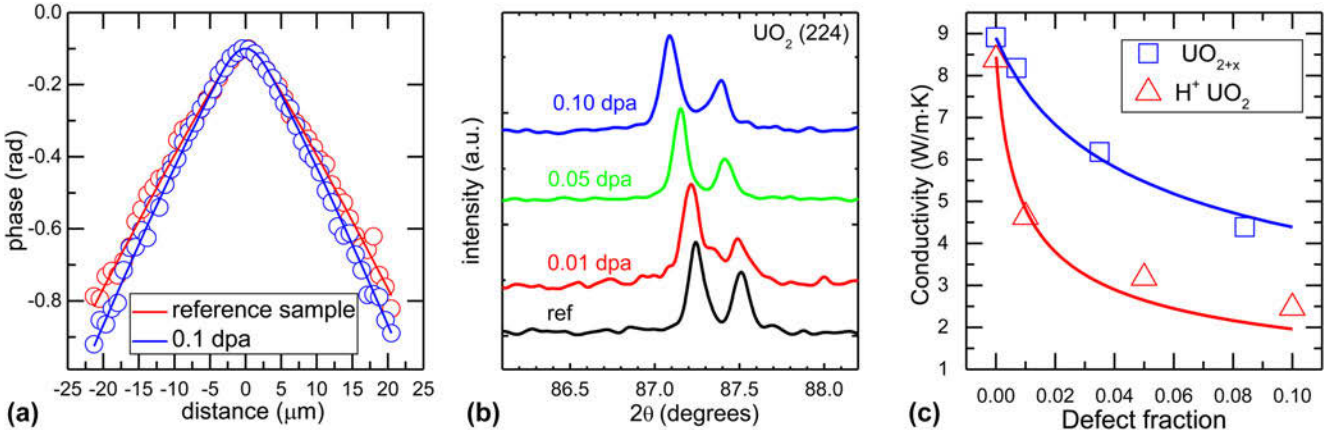

FIG. 2. Measurement of thermal conductivity in proton irradiated UO_2. (a) Thermal wave profiles measured at 2 kHz, symbols are experimental data and solid lines are model fits, (b) XRD patterns from Ref. 42 showing defect accumulation, and (c) measured thermal conductivity is compared to nonstoichiometric values from Ref. 50, solid line are fit to a model.

were assumed to be uniform. This multilayer model was used to choose the appropriate modulation frequency that is most sensitive to the plateau damage and least sensitive to the peak damage region in our studies.

Figure 2(b) summarizes x-ray diffraction (XRD) diffraction analysis of the irradiated sample.[42] Well-defined peaks [only (224) peak is shown] indicate that the samples remained crystalline after the irradiation. A gradual peak shift to a smaller angle with increasing dose indicates lattice expansion due to accumulation of point defects.[51] This is in agreement with previous work in He ion irradiated UO_2, but in contrast with shrinkage of the lattice when O interstitials are present in nonstoichiometric UO_{2+x}.[23,52,53]

The thermal conductivity values obtained from the analysis of measured thermal wave profiles are summarized in Fig. 2(c). It shows a gradual decrease of thermal conductivity as the damage increases, as expected. We compare our results qualitatively against conductivity values for the nonstoichiometric UO_{2+x}, where the primary defects are oxygen interstitials.[50,54] The comparison is done versus concentration of defects per unit cell. It is concentration of oxygen interstitials (i.e., value of x in UO_{2+x} and dpa value for the irradiated sample). It is clear that this comparison suggests that defects resulting from H^+ irradiation cause a stronger reduction in conductivity. This can be attributed to the fact that displacement damage in addition to oxygen defects generates uranium defects that are not available in nonstoichiometric samples. There is also an indication that U lattice defects have a stronger phonon scattering cross-section.[23,55] In the above discussion, we neglected the contribution of implanted H^+ atoms due their much lower concentration compared to generated point defects.

The reduction of thermal conductivity was analyzed quantitatively using the classical thermal transport model based on Klemens–Callaway formalism that accounts for intrinsic factors limiting heat transport and irradiation induced point defects.[56] The phonon scattering cross-section is used to quantify the impact of point defects on conductivity of materials whose thermal transport is governed by lattice vibrations. The defect's scattering cross-section is defined by two parameters, a mass mismatch and ionic radius mismatch.[57] Based on ab initio calculation, uranium-based defects have larger relaxation volumes and thus are expected to have a larger impact on thermal conductivity, consistent with our qualitative analysis.[55]

B. Impact of dislocation loops on thermal conductivity

Impact of dislocation loops on thermal transport in ceramic materials was studied in CeO_2, which was used as a surrogate for UO_2. Two CeO_2 samples sliced from commercially available sintered pellets (Alfa Aesar) were irradiated at $T = 700$ °C using 1.6 MeV protons derived from a NEC Pelletron Tandem accelerator to a fluence of 2.8×10^{18} and 1.4×10^{19} ions/cm^2.[40] SRIM software calculations were performed using the displacement energies of 20 eV and 40 eV for O and Ce, respectively. It was found using the SRIM calculations that the plateau region was confined to the top 16 μm, the higher fluence produced a damage of ~1.0 dpa and the lower fluence led to a damage of ~0.2 dpa. The plateau region is followed by 2 μm thick layer having significantly higher damage than the plateau region. Similar to the previously described UO_2 example, the irradiated zone was approximated by two layers with uniform damage.

Specific to this study, thermal wave profiles were excited by a 400 nm wave length pump beam and

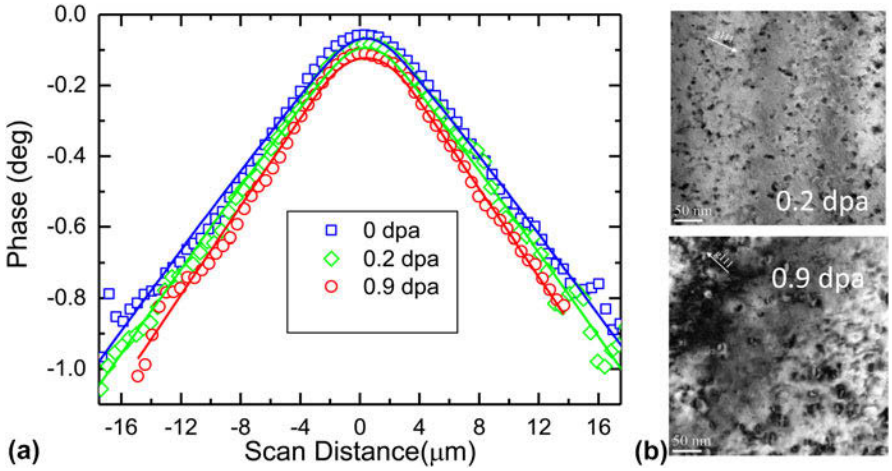

FIG. 3. (a) Thermal wave profile measured hydrogen ion irradiated CeO_2 samples. Experimental data are represented by individual data points and solids lines are fits to the model used to extract thermal conductivity. Thermal profiles from top to bottom have increasing slope, corresponding to decreasing thermal conductivity, as we go from as-received sample down to irradiated samples. (b) Electron microscopy images depicting dislocation loops.

sensed by a 800 nm wave length probe beam and the samples were coated with a 50 nm thick aluminum layer. Typical thermal wave profiles measured using this configuration are plotted in Fig. 3. Again we see that thermal wave develops a phase lag with respect to the excitation and the phase profile has a linear dependence sufficiently away from the pump. As in the case of H^+ irradiated UO_2, we see that irradiated CeO_2 exhibits a larger slope, as compared to the reference. However in this case, due to a significantly higher irradiation temperature, the reduction is expected to be due to extended defects.[58,59]

Irradiation damage was characterized using transmission electron microscopy (TEM). Figure 3(b) shows representative TEM micrographs which clearly reveal the presence of irradiation induced dislocation loops in both samples. As expected, the high irradiation dose sample contains larger loops and higher loop density. The dislocation loop average radius R_d and volume density n_d were determined by analyzing a series of TEM micrographs and are listed in Table I. Additionally x-ray diffraction analysis was performed to assess the damage. In this high-temperature irradiated CeO_2, lattice expansion caused by point defect accumulation was minimal. This is in contrast to the observation of substantial lattice expansion due to point defects in low temperature irradiated UO_2. Analysis based on classical thermal transport models suggests that dislocation loops have a significant impact on thermal conductivity reduction in this sample.[12,60,61]

TABLE I. Characterization summary of proton irradiated CeO_2.

	Reference	0.2 dpa	0.9 dpa
Dislocation loop radius, R (nm)	...	3.7 ± 1.1	7.4 ± 2.0
Dislocation loop density, n_d (10^{21} m^{-3})	...	3.9 ± 0.2	6.1. ± 1.2
Thermal conductivity, κ (W/m K)	24.9	21.7	19.6

C. Impact of fission products on thermal conductivity

Fission gas products were introduced by implanting Kr ion using an ion accelerator. Kr ions were accelerated to 1 MeV energy using a Van der Graaff accelerator at University of Illinois Urbana Champaign and implanted into cubic 3C-silicon carbide (SiC) under varying temperature and fluence.[41] 3C-SiC were obtained from a commercial vendor (Cree). We summarize this study by presenting the result on 3 samples.[41] Sample (A) is an as-received sample and is used as a reference. Sample (B) was irradiated at 50 °C and an estimated dose of 0.004 dpa. Sample (C) was irradiated at room temperature to an estimated dose of 0.4 dpa. SRIM calculation suggests this implantation configuration resulted in a damage profile confined to 600 nm. This is too shallow for SDTR to be sensitive to the damaged layer; therefore, we used TDTR for its greater sensitivity to the near surface region of the sample.[62] Compared to SDTR, TDTR uses a much higher modulation frequency for the pump beam (on the order of few MHz compared to SDTR's few tens of kHz). For these high frequencies, the thermal wave amplitude decays rapidly away from the heater and the spatial domain measurement becomes impractical. This short thermal wave length associated with TDTR introduces one limitation which is related to the influence of surface roughness. The impact of surface roughness becomes especially pronounced in ion irradiated samples.[63] This manifests itself as a large error bar in our analysis presented below.

Figure 4(a) depicts typical transients measured in Kr irradiated SiC. In TDTR, it is more convenient to

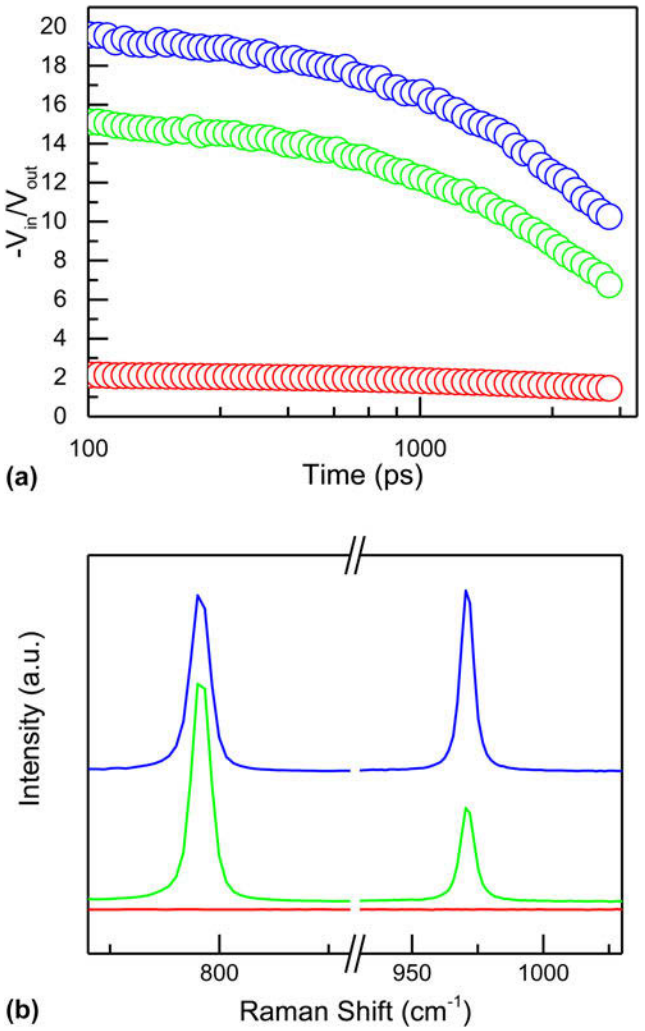

FIG. 4. Measurement of thermal conductivity in krypton irradiated SiC. (a) Time domain thermal wave profiles. (b) Raman spectra of the samples.

analyze the ratio between in-phase and out-phase components of the temperature (V_{in}/V_{out}). The cotangent of V_{in}/V_{out} is equivalent to the phase. Typically values of V_{in}/V_{out} are larger for a material whose conductivity is larger. Qualitative analysis suggests that the reference sample-A has the largest conductivity of 360 ± 20 W/m K, sample B has a lower conductivity of 260 ± 70 W/m K, and sample C has a very low conductivity 1.6 ± 0.3 W/m K. Based on previous reports, sample B underwent a minor defect accumulation, whereas sample C was amorphized.[12]

The same set of samples was characterized using confocal Raman spectroscopy. The spectral region corresponding to two major peak E_1(TO) and A_1(LO) at 795 cm^{-1} and 970 cm^{-1},[64,65] respectively, are shown in Fig. 4(b). While these peaks are present in both A and B, they are absent in C. This indicates that sample B retained its crystalline structure while sample C completely amorphized, consistent with thermal conductivity data. Close examination of the spectra in sample B reveals a different magnitude for the ratio of the intensities of two peaks, when compared to the reference. While the intensity of the peak I_{972}/I_{796} in the reference sample is about 1, it is about 0.6 in sample B. This can be attributed to the fact that A_1(LO) is more sensitive to specific types of defects than E_1(TO).[66]

D. Importance of irradiation damage on thermal conductivity

The current state of the advanced computational tools allows development of fuel performance codes that are based on the atomic level first principle calculations and capture physical phenomena across multiple scales.[17] Unlike current fuel performance codes which are essentially empirical models that are based on a limited set of experimental data, first principles based codes are expected to have predictive capability. This predictive capability of fuel performance codes is very important for understanding the fuel behavior under conditions beyond normal operation.

Importance of atomic level calculations can also be rationalized by realizing that many fundamental physical processes taking place in the fuel during service are very hard to quantify experimentally. In fact, most of the physical parameters used in the models are actually inferred from post irradiation experimental measurements that are prone to misrepresent the actual condition of the fuel in service. In light of this, a number of activities have recently been initiated focusing on the development of lower length scale modeling tools for describing the performance of UO_2 fuel.[67,68] They aim at incorporating physical mechanisms at both atomic and mesoscale levels to capture phenomena such as grain growth and fission gas bubbles evolution. For instance, thermal conductivity model includes reduction of thermal conductivity combining microstructure features across multiple scales due to formation of fission gas bubbles, beginning from the moment fission atoms can be treated as point defects and subsequently evolving into bubbles that may arrange themselves along grain boundaries.[19] In addition to the fission gases, the effect of nonstoichiometry and Frenkel pairs on thermal conductivity is also important.[43,69] These types of defects may exist under the presence of radiation flux and are absent in standard post irradiation examination.

While these lower scale codes are being developed, it is realized that there is a need to experimentally validate these models.[70] The results of the work presented above demonstrate the attractiveness of experimental studies combining ion beam irradiations, TR methods, and microstructure characterization techniques including x-ray diffraction, Raman spectroscopy, and electron microscopy techniques to validate the specific aspects of these efforts.[24,38]

IV. MEASUREMENT IN COMPOSITES

In this section, we present the results of measurement of thermal transport in composite materials, including tristructural isotropic (TRISO) particle fuel, SiC/SiC fiber composites, and 2nd phase precipitates in intermetallic fuels. We also distinguish between two different types of measurements. First is to determine conductivity of each individual layer or component and in the second, we focus on the measurement of thermal interface resistance between two layers.

A. TRISO fuel particle

TRISO-coated particle is a form of fuel that has been developed for over five decades and demonstrated in high-temperature gas-cooled reactors in many countries.[71] Its primary design characteristic is to contain radioactive fission products within its layered structure. It consisted of fuel kernel, graphite buffer, inner pyrolytic carbon (IPyC) layer, SiC layer, and outer pyrolytic carbon (OPyC) layer. The porous graphite buffer absorbs fission products while SiC layer provides the main structural support and barrier for fission products. PyC layers provide additional mechanical support, retain fission products and protect the fuel kernel from erosive gas during deposition. Conventionally, the kernel is made by a sol–gel process and coating is achieved through a series of fluidized-bed coaters, whereas different countries have made various modifications resulting in different performances.[72] Tests showed that TRISO fuel can maintain structural integrity, withstand irradiation and very high temperature up to 1000 °C.[73] Extensive post irradiation examinations were done to characterize mechanical properties, chemical composition change, fission gas leakage, etc. to provide feedback to fuel fabrication and modeling.[73,74] Mechanical interaction between layers has an impact on integrity of TRISO fuel particle, ultimately impacting its fission product retention characteristics. The ability to assess fission product retention and mechanical integrity of the fuel relies on the knowledge of temperature distribution which requires determining the conductivity for individual layers.[75,76]

In this study we measured thermal conductivity of each layer using a surrogate fuel compact whose fuel kernel was replaced by zirconia. An optical micrograph of a particle sliced approximately along its equator is shown in Fig. 5(a). Individual layers are clearly seen and identified in the graph. The thickness of each layer varies between few tens of micrometers to a hundred microns. Each layer is sufficiently thick so that the probe scan was confined to a single layer while the pump was located at center. For very thin layers, thermal wave profiles were measured along the circumferential direction. Therefore, the measured profiles could have been impacted by the neighboring layers. However, our analysis suggests this effect is minimal as long as the pump beam is several μm away from the interface.

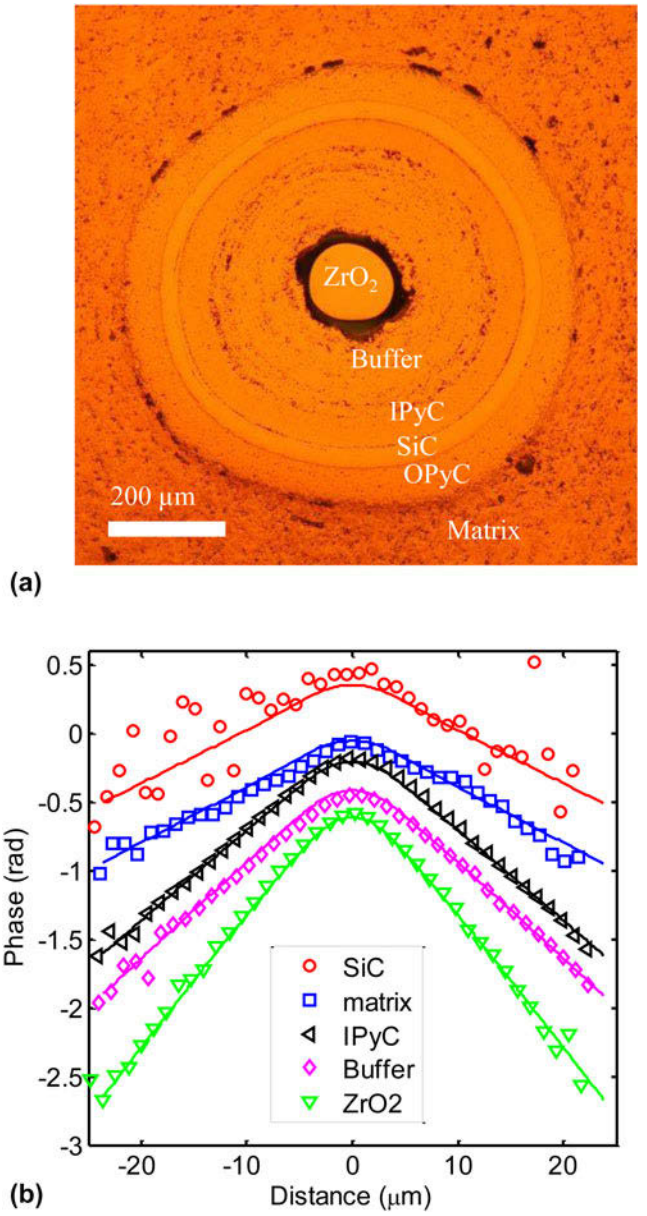

FIG. 5. Measurement in TRISO fuel. (a) Optical image of the TRISO fuel with a layered structure. (b) Thermal wave profiles measured from selected layers. Symbols are experimental data and solid lines are model fits used to measure thermal conductivity.

Thermal wave profiles measured from each individual layer are shown in Fig. 5(b). The variation of the slope clearly indicates different thermal properties for each layer. The extracted thermal conductivity values are summarized in Table II and compared to a previous work[77] and values used in PARFUME fuel performance code.[78] We see a reasonable agreement between our and previously published results with the exception of buffer layer. The buffer layer is highly porous and our measurement corresponds to its skeleton conductivity, thus is

the large discrepancy. In principle, the approach can be extended to measure the thermal interface resistance between different layers to assess the impact of debonding on thermal transport.

B. 2nd phase precipitates

Here, we present spatially resolved measurement of thermal conductivity in a U_3Si_2 fuel surrogate. U_3Si_2 is considered as an alternative fuel to UO_2 due to its higher uranium atom density and thermal conductivity.[79] Unlike previously discussed cases, the conductivity of this material is determined by electron transport. Point defects and extended defects do not typically have a strong impact on electronic thermal conductivity, unless the material is cooled to cryogenic temperatures.[80,81] Currently, U_3Si_2 is used as a fuel in research reactor, where operating temperatures are lower, but the fuel is exposed to higher burn-up. Recently, efforts have been initiated to understand the behavior of this material under irradiation conditions representative of commercial nuclear reactors. Under light water reactor conditions, the fuel temperature is expected to be higher than research reactor conditions. This raises several questions concerning microstructure evolution. From a thermal conductivity perspective, the primary concern is swelling and emergence of 2nd phase precipitates, as opposed to point defects or extended defect as is the case with oxide or silicon carbide.[80]

We show the ability of TR to resolve the conductivity of 2nd phase precipitates. For this demonstration, a sample was chosen that contains 2nd phase precipitates developed during the fabrication process and identified as the oxide phase of uranium.[39] For this purpose we used the time domain version of the TR setup, where the sample is excited by a square wave modulation. This is achieved by direct electrical triggering of a continuous wave diode laser. Unlike frequency or spatial domain measurements where one measures the phase of the thermal wave profile, here we directly monitor the temporal evolution of signal detected on the photodiode, corresponding to a temperature transient on the surface of the samples. The data analysis resembles that of TDTR, however this approach uses square wave excitation whereas TDTR uses delta function excitation. Figure 6 shows typical transients observed from two different points on the surface of the sample. The signal is characterized by a truncated square wave, similar to the behavior observed when a square wave is sent through a low pass filter. In this configuration, it is expected that materials with higher thermal conductivity exhibits a shorter time constant.

We see that the response of the matrix is faster, indicating that the precipitate has a smaller conductivity than the matrix. This suggests that emergence of irradiation induced 2nd phase precipitate can have an impact on thermal conductivity of U_3Si_2 and this approach could be used to further analyze this behavior on irradiated materials.

TABLE II. Thermal conductivity of TRISO particle layers.

	Current work (W/m K)	PARFUME[78] (W/m K)	Rochais[77] (W/m K)
Matrix	26.2 ± 0.9	39.7	...
OPyC	6.7 ± 0.3	4	4.8
SiC	62.1 ± 1.7	61	NA
IPyC	8.4 ± 0.1	4	10.3
Buffer	6.5 ± 0.1	0.5	7.0
ZrO_2	3.1 ± 0.5	...	2.3

C. SiC fiber composites

Silicon carbide is an attractive ceramic material for nuclear applications due to its high melting temperature, chemical inertness, and mechanical hardness.[82] It exhibits resistance to radiation over a broad temperature range above room temperature, where radiation induced swelling is minimal.[83] Like most ceramics SiC is brittle, making it impractical for general applications in its bulk form.

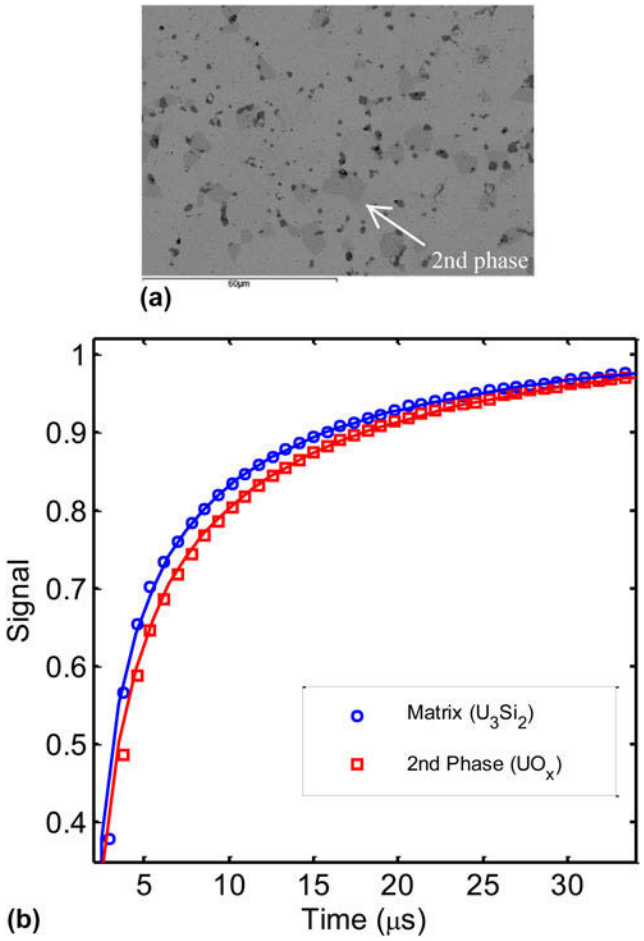

FIG. 6. Measurement in U_3Si_2 fuel. (a) SEM image from Ref. 39. (b) Time resolved thermal wave profiles measured from matrix (7.1 W/m K) and 2nd phase precipitate (5.9 W/m K).

However, issues associated with brittleness are mitigated when used in a composite form where SiC fibers (SiC_f) are embedded in SiC matrix (SiC_m).[84] Mechanical strength of the composite is enhanced by introducing a thin pyrolytic carbon interphase layer that acts as a barrier for crack propagation under embrittlement conditions.[85]

While the properties of bulk SiC and its radiation behavior were extensively studied, the behavior of this ceramic matrix composite (CMC) is an active area of research.[86] Our specific focus here is to understand thermal transport in this composite material. TR techniques offer the capability to measure thermal properties of the matrix and fiber separately. More importantly it can be used to assess thermal interface resistance, which could be large due to the presence of the PyC interphase layer and debonding.

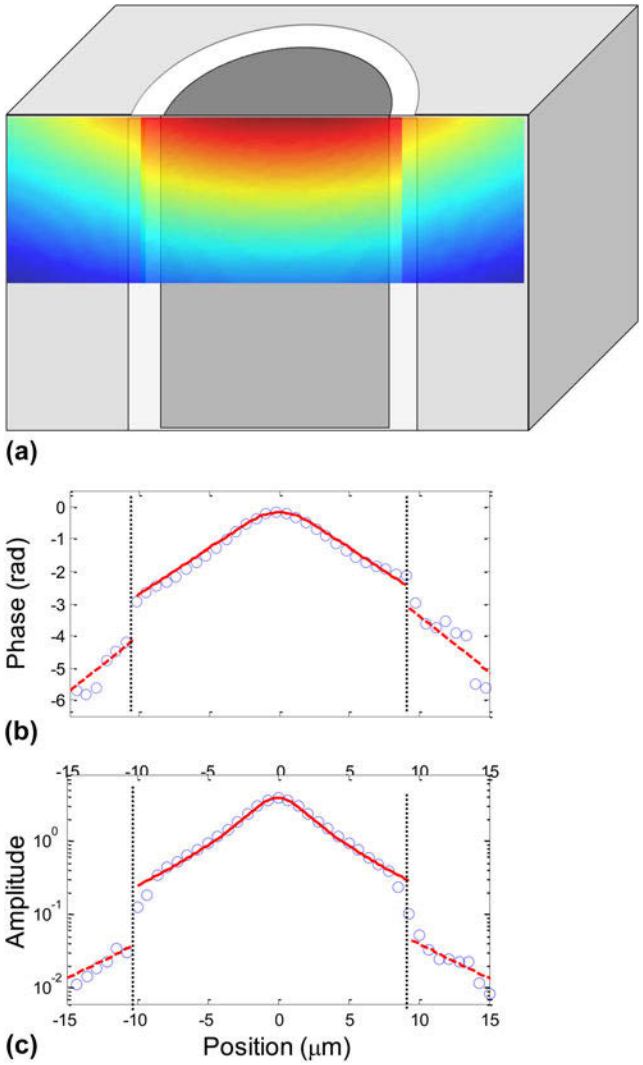

FIG. 7. Spatially resolved measurement of thermal transport in SiC fiber composites. (a) Schematics of the measured thermal wave when the pump is parked at the center of the fiber. (b) Phase and (c) amplitude profiles of the measured thermal waves. Symbols are experimental data and solid lines are modeled profiles. The step change in phase and amplitude is due to thermal interface resistance between two layers.

Figure 7 summarizes the result of our spatially resolved study on CMC based on Nicalon Type S fibers.[87] The bulk composite material was polished in such way that a fiber is aligned normal to the surface. The diameter of the fiber is about 20 μm. The pump is focused at the center of the fiber and the probe is scanned on the surface to map the thermal wave profile. This configuration is similar to a study on Si bicrystal interface[88] reported previously and implements 400 nm pump and 800 nm probe beams based on Ti:sapphire femtosecond laser. One notable difference from Ref. 88 is that for current measurement it was necessary to deposit a thin Al film.

A representative profile for both phase and amplitude is shown in Fig. 7. The phase profiles within each individual layer are characterized by a linear dependence. These linear sections are analyzed to extract thermal conductivity for SiC_f and SiC_m. The fiber conductivity was found to be 19 ± 2 W/m K and matrix conductivity varied in the range 13–24 W/m K. We observe an additional phase lag acquired by the thermal wave as it crosses the interface due to interface thermal resistance. This interface resistance also manifests itself in the amplitude profile which exhibits a noticeable drop in its intensity across the interface. Such a noticeable impact of interface resistance is attributed to the presence of an additional PyC interphase layer that acts as a barrier for heat transport. The ability to measure thermal conductivity of each layer and interface resistance in composite materials opens up a possibility to improve our understanding of thermal transport in irradiated CMC composites.[86]

D. Practical considerations for implementation of TR techniques

In this section, we discuss the requirements for surface preparation and limitations of the TR approaches. Successful implementation of the TR methods relies on the ability to obtain optically flat surfaces in samples under investigation. This is required not only to ensure optimal reflection of the probe beam but also to satisfy the thermally flat surface assumption used in the heat diffusion model.[33] This becomes of particular concern in the TDTR measurements where high frequency modulation of the pump results in very shallow penetration of thermal waves that can be comparable to the surface roughness.[63] Optically flat surface can be achieved by implementing surface polishing techniques used in preparation of samples for characterization under scanning electron microscopes.

In case of ion beam damaged samples, an additional consideration is that if irradiation is not conducted properly it results in the surface roughness and the

sample cannot be polished as this would remove the damage layer. Therefore, ion irradiation experiments need to be performed under optimal conditions otherwise resulting samples are not suitable for TR measurements. Thus far this has been the primary obstacle in our efforts related to UO_2 work. In the experiments that focus on measuring interface thermal resistance, special care should be given to surface preparation as well. For these studies, it is critical to avoid development of surface topography around the interface during polishing.[88]

It should be realized that while TR approaches are effective in providing conductivity measurements with several micron resolution, they are not appropriate for investigations that require measurement of thermal properties averaged over tens of microns such as the effective conductivity of SiC fiber composites or highly porous materials. For these applications, one would rely on laser flash apparatus or infrared pyrometry.[77]

V. CONCLUSIONS

We have presented several examples demonstrating the application of TR techniques to provide spatially resolved measurement of thermal transport in nuclear materials. This technique is attractive for validation of atomic and mesoscale models and is expected to provide important input for the next generation of fuel performance codes. An important feature of TR techniques discussed in this paper is that they can be used to measure the influence of ion irradiation damage on thermal conductivity. Ion beam irradiation conditions can be tailored to study the impact of atomic level defects such as Frenkel pairs, small defect clusters, higher order defects, including dislocations, voids, bubbles, and 2nd phase precipitates. TR techniques can also be applied to measure the individual response of elements that form composite materials. Here, micron scale resolution allows measurement of thermal conductivity of each individual layer and thermal interface resistance between layers.

ACKNOWLEDGMENTS

Authors would like to acknowledge Andrew Nelson, Jason Harp, Paul Demkowicz, and Yutai Katoh for providing various samples, Xinpeng Du and Changdong Wei for assistance with TDTR measurements, and Janne Pakarinen, Beata Tyburska-Puschel, and Lingfeng He with assistance on ion beam irradiations and microstructure characterization.

REFERENCES

1. D.R. Olander: *Fundamental Aspects of Nuclear Reactor Fuel Elements: Prepared for the Division of Reactor Development and Demonstration, Energy Research and Development Administration* (Technical Information Center, Office of Public Affairs, Springfield, VA, 1976).
2. T.L. Bergman and F.P. Incropera: *Fundamentals of Heat and Mass Transfer*, 7th ed. (Wiley, Hoboken, 2011).
3. J.R. Lamarsh and A.J. Baratta: *Introduction to Nuclear Engineering*, 3rd ed. (Prentice Hall, Upper Saddle River, 2001).
4. G.S. Was: *Fundamentals of Radiation Materials Science: Metals and Alloys* (Springer, Berlin, 2007).
5. C. Ronchi, M. Sheindlin, D. Staicu, and M. Kinoshita: Effect of burn-up on the thermal conductivity of uranium dioxide up to 100.000 MWdt(−1). *J. Nucl. Mater.* **327**(1), 58 (2004).
6. K. Lassmann: TRANSURANUS—A fuel-rod analysis code ready for use. *J. Nucl. Mater.* **188**, 295 (1992).
7. K. Geelhood, W.G. Luscher, and C.E. Beyer: *FRAPCON-3.4: A Computer Code for the Calculation of Steady State Thermal-Mechanical Behavior of Oxide Fuel Rods for High Burnup* (NRC, Washington, DC, 2011).
8. R.L. Williamson, J.D. Hales, S.R. Novascone, M.R. Tonks, D.R. Gaston, C.J. Permann, D. Andrs, and R.C. Martineau: Multidimensional multiphysics simulation of nuclear fuel behavior. *J. Nucl. Mater.* **423**(1–3), 149 (2012).
9. T.M. Tritt: *Thermal Conductivity: Theory, Properties, and Applications* (Kluwer Academic/Plenum Publishers, New York, 2004).
10. C. Jensen, C. Xing, C. Folsom, H. Ban, and J. Phillips: Design and validation of a high-temperature comparative thermal-conductivity measurement system. *Int. J. Thermophys.* **33**(2), 311 (2012).
11. A. Cezairliyan, T. Baba, and R. Taylor: A high-temperature laser-pulse thermal diffusivity apparatus. *Int. J. Thermophys.* **15**(2), 317 (1994).
12. L.L. Snead, S.J. Zinkle, and D.P. White: Thermal conductivity degradation of ceramic materials due to low temperature, low dose neutron irradiation. *J. Nucl. Mater.* **340**(2–3), 187 (2005).
13. C. Ronchi, M. Sheindlin, M. Musella, and G.J. Hyland: Thermal conductivity of uranium dioxide up to 2900 K from simultaneous measurement of the heat capacity and thermal diffusivity. *J. Appl. Phys.* **85**(2), 776 (1999).
14. J.J. Powers and B.D. Wirth: A review of TRISO fuel performance models. *J. Nucl. Mater.* **405**(1), 74 (2010).
15. K.A. Terrani, J.O. Kiggans, Y. Katoh, K. Shimoda, F.C. Montgomery, B.L. Armstrong, C.M. Parish, T. Hinoki, J.D. Hunn, and L.L. Snead: Fabrication and characterization of fully ceramic microencapsulated fuels. *J. Nucl. Mater.* **426**(1–3), 268 (2012).
16. V.V. Rondinella and T. Wiss: The high burn-up structure in nuclear fuel. *Mater. Today* **13**(12), 24 (2010).
17. J.Y.R. Rashid, S.K. Yagnik, and R.O. Montgomery: Light water reactor fuel performance modeling and multi-dimensional simulation. *JOM* **63**(8), 84 (2011).
18. M. Bertolus, M. Freyss, B. Dorado, G. Martin, K. Hoang, S. Maillard, R. Skorek, P. Garcia, C. Valot, A. Chartier, L. Van Brutzel, P. Fossati, R.W. Grimes, D.C. Parfitt, C.L. Bishop, S.T. Murphy, M.J.D. Rushton, D. Staicu, E. Yakub, S. Nichenko, M. Krack, F. Devynck, R. Ngayam-Happy, K. Govers, C.S. Deo, and R.K. Behera: Linking atomic and mesoscopic scales for the modelling of the transport properties of uranium dioxide under irradiation. *J. Nucl. Mater.* **462**, 475 (2015).
19. M.R. Tonks, X-Y. Liu, D. Andersson, D. Perez, A. Chernatynskiy, G. Pastore, C.R. Stanek, and R. Williamson: Development of a multiscale thermal conductivity model for fission gas in UO_2. *J. Nucl. Mater.* **469**, 89 (2016).
20. G.S. Was and T.R. Allen: Radiation damage from different particle types. In *Radiation Effects in Solids*, Springer: Netherlands, 2007; p. 65.
21. M.P. Short, C.A. Dennett, S.E. Ferry, Y. Yang, V.K. Mishra, J.K. Eliason, A. Vega-Flick, A.A. Maznev, and K.A. Nelson:

Applications of transient grating spectroscopy to radiation materials science. *JOM* **67**(8), 1840 (2015).
22. F. Hofmann, D.R. Mason, J.K. Eliason, A.A. Maznev, K.A. Nelson, and S.L. Dudarev: Non-contact measurement of thermal diffusivity in ion-implanted nuclear materials. *Sci. Rep.* **5**, 1–7 (2015).
23. J. Pakarinen, M. Khafizov, L. He, C. Wetteland, J. Gan, A.T. Nelson, D.H. Hurley, A. El-Azab, and T.R. Allen: Microstructure changes and thermal conductivity reduction in UO_2 following 3.9 MeV He^{2+} ion irradiation. *J. Nucl. Mater.* **454**(1–3), 283 (2014).
24. R. Cheaito, C.S. Gorham, A. Misra, K. Hattar, and P.E. Hopkins: Thermal conductivity measurements via time-domain thermoreflectance for the characterization of radiation induced damage. *J. Mater. Res.* **30**(9), 1403 (2015).
25. R. Allan, O. Jon, W.L. Smith, and D.L. Willenborg: Detection of thermal waves through optical reflectance. *Appl. Phys. Lett.* **46**(11), 1013 (1985).
26. R.B. Wilson, B.A. Apgar, L.W. Martin, and D.G. Cahill: Thermoreflectance of metal transducers for optical pump-probe studies of thermal properties. *Opt. Express* **20**(27), 28829 (2012).
27. A.P. Carolyn and L.E. Gary: Transient thermoreflectance from thin metal films. *J. Appl. Phys.* **60**(1), 285 (1986).
28. D.G. Cahill: Analysis of heat flow in layered structures for time-domain thermoreflectance. *Rev. Sci. Instrum.* **75**(12), 5119 (2004).
29. W.S. Capinski and H.J. Maris: Improved apparatus for picosecond pump-and-probe optical measurements. *Rev. Sci. Instrum.* **67**(8), 2720 (1996).
30. D.G. Cahill, W.K. Ford, K.E. Goodson, G.D. Mahan, A. Majumdar, H.J. Maris, R. Merlin, and S.R. Phillpot: Nanoscale thermal transport. *J. Appl. Phys.* **93**(2), 793 (2003).
31. Z.L. Hua, H. Ban, M. Khafizov, R. Schley, R. Kennedy, and D.H. Hurley: Spatially localized measurement of thermal conductivity using a hybrid photothermal technique. *J. Appl. Phys.* **111**(10), 7 (2012).
32. J.A. Malen, K. Baheti, T. Tong, Y. Zhao, J.A. Hudgings, and A. Majumdar: Optical measurement of thermal conductivity using fiber aligned frequency domain thermoreflectance. *J. Heat Transfer* **133**(8), 7 (2011).
33. M. Khafizov and D.H. Hurley: Measurement of thermal transport using time-resolved thermal wave microscopy. *J. Appl. Phys.* **110**(8), 083525 (2011).
34. A.A. Maznev, J. Hartmann, and M. Reichling: Thermal-wave propagation in thin-films on substrates. *J. Appl. Phys.* **78**(9), 5266 (1995).
35. L. David, S. Gomes, G. Carlot, J.P. Roger, D. Fournier, C. Valot, and M. Raynaud: Characterization of thermal conductivity degradation induced by heavy ion irradiation in ceramic materials. *J. Phys. D: Appl. Phys.* **41**(3), 035502 (2008).
36. D.H. Hurley, R.S. Schley, M. Khafizov, and B.L. Wendt: Local measurement of thermal conductivity and diffusivity. *Rev. Sci. Instrum.* **86**(12), 123901 (2015).
37. D.H. Hurley, O.B. Wright, O. Matsuda, and S.L. Shinde: Time resolved imaging of carrier and thermal transport in silicon. *J. Appl. Phys.* **107**(2), 5 (2010).
38. M. Khafizov, C. Yablinsky, T.R. Allen, and D.H. Hurley: Measurement of thermal conductivity in proton irradiated silicon. *Nucl. Instrum. Methods Phys. Res., Sect. B.* **325**, 11 (2014).
39. J.M. Harp, P.A. Lessing, and R.E. Hoggan: Uranium silicide pellet fabrication by powder metallurgy for accident tolerant fuel evaluation and irradiation. *J. Nucl. Mater.* **466**, 728 (2015).
40. M. Khafizov, J. Pakarinen, L. He, C. Yablinsky, T.R. Allen, and D.H. Hurley: Impact of irradiation induced dislocation loops on thermal conductivity. Unpublished manuscript.
41. V.S. Chauhan, M.F. Riyad, X. Du, C. Wei, J.C. Zhao, B. Tyburska-Püschel, and M. Khafizov: Impact of radiation damage on thermal conductivity and Raman spectra in low dose ion irradiated 3C-SiC. Submitted to *Metall. Mater. Trans. E.*
42. J. Pakarinen, L. He, M. Gupta, J. Gan, A. Nelson, A. El-Azab, and T.R. Allen: 2.6 MeV proton irradiation effects on the surface integrity of depleted UO_2. *Nucl. Instrum. Methods Phys. Res., Sect. B.* **319**, 100 (2014).
43. T. Watanabe, S.G. Srivilliputhur, P.K. Schelling, J.S. Tulenko, S.B. Sinnott, and S.R. Phillpot: Thermal transport in off-stoichiometric uranium dioxide by atomic level simulation. *J. Am. Ceram. Soc.* **92**(4), 850 (2009).
44. J-P. Crocombette and L. Proville: Thermal conductivity degradation induced by point defects in irradiated silicon carbide. *Appl. Phys. Lett.* **98**(19), 191905 (2011).
45. P.C. Millett, M.R. Tonks, K. Chockalingam, Y. Zhang, and S.B. Biner: Three dimensional calculations of the effective Kapitza resistance of UO_2 grain boundaries containing intergranular bubbles. *J. Nucl. Mater.* **439**(1–3), 117 (2013).
46. C.W. Lee, A. Chernatynskiy, P. Shukla, R.E. Stoller, S.B. Sinnott, and S.R. Phillpot: Effect of pores and He bubbles on the thermal transport properties of UO_2 by molecular dynamics simulation. *J. Nucl. Mater.* **456**, 253 (2015).
47. B. Valderrama, L.F. He, H.B. Henderson, J. Pakarinen, B. Jaques, J. Gan, D.P. Butt, T.R. Allen, and M.V. Manuel: Effect of grain boundaries on krypton segregation behavior in irradiated uranium dioxide. *JOM* **66**(12), 2562 (2014).
48. L.F. He, B. Valderrama, A.R. Hassan, J. Yu, M. Gupta, J. Pakarinen, H.B. Henderson, J. Gan, M.A. Kirk, A.T. Nelson, M.V. Manuel, A. El-Azab, and T.R. Allen: Bubble formation and Kr distribution in Kr-irradiated UO_2. *J. Nucl. Mater.* **456**, 125 (2015).
49. R.E. Stoller, M.B. Toloczko, G.S. Was, A.G. Certain, S. Dwaraknath, and F.A. Garner: On the use of SRIM for computing radiation damage exposure. *Nucl. Instrum. Methods Phys. Res., Sect. B.* **310**, 75 (2013).
50. J.T. White and A.T. Nelson: Thermal conductivity of UO_{2+x} and U_4O_{9-y}. *J. Nucl. Mater.* **443**(1–3), 342 (2013).
51. W.J. Weber: Ingrowth of lattice-defects in alpha irradiated UO_2 single crystals. *J. Nucl. Mater.* **98**(1–2), 206 (1981).
52. L. Lynds, W.A. Young, J.S. Mohl, and G.G. Libowitz: An X-ray and density study of nonstoichiometry in uranium oxides. In *Nonstoichiometric Compounds*; American Chemical Society: Washington, DC, 1963; p. 58.
53. W.J. Weber: Alpha-irradiation damage in CeO_2, UO_2 and PuO_2. *Radiat. Eff. Defects Solids* **83**(1–2), 145 (1984).
54. P.G. Lucuta, H. Matzke, and R.A. Verrall: Thermal conductivity of hyperstoichiometric SIMFUEL. *J. Nucl. Mater.* **223**(1), 51 (1995).
55. H.Y. Geng, H.X. Song, K. Jin, S.K. Xiang, and Q. Wu: First-principles study on oxidation effects in uranium oxides and high-pressure high-temperature behavior of point defects in uranium dioxide. *Phys. Rev. B: Condens. Matter Mater. Phys.* **84**(17), 104120 (2011).
56. P.G. Klemens: Thermal conductivity and lattice vibration modes. *Solid State Phys.* **7**, 1 (1958).
57. B. Abeles: Lattice thermal conductivity of disordered semiconductor alloys at high temperatures. *Phys. Rev.* **131**(5), 1906 (1963).
58. L.F. He, M. Gupta, M.A. Kirk, J. Pakarinen, J. Gan, and T.R. Allen: In situ TEM observation of dislocation evolution in polycrystalline UO_2. *JOM* **66**(12), 2553 (2014).
59. B. Ye, M.A. Kirk, W. Chen, A. Oaks, J. Rest, A. Yacout, and J.F. Stubbins: TEM investigation of irradiation damage in single crystal CeO_2. *J. Nucl. Mater.* **414**(2), 251 (2011).
60. M. Khafizov, I.W. Park, A. Chernatynskiy, L.F. He, J.L. Lin, J.J. Moore, D. Swank, T. Lillo, S.R. Phillpot, A. El-Azab, and

D.H. Hurley: Thermal conductivity in nanocrystalline ceria thin films. *J. Am. Ceram. Soc.* **97**(2), 562 (2014).
61. P.G. Klemens: Theory of thermal conductivity in dielectric solids —Effects of radiation damage. *Nucl. Instrum. Methods Phys. Res., Sect. B.* **1**(2–3), 204 (1984).
62. C. Wei, X. Zheng, D.G. Cahill, and J-C. Zhao: Invited article: Micron resolution spatially resolved measurement of heat capacity using dual-frequency time-domain thermoreflectance. *Rev. Sci. Instrum.* **84**(7), 071301 (2013).
63. P.B. Weisensee, J.P. Feser, and D.G. Cahill: Effect of ion irradiation on the thermal conductivity of UO_2 and U_3O_8 epitaxial layers. *J. Nucl. Mater.* **443**(1–3), 212 (2013).
64. S. Nakashima and H. Harima: Raman investigation of SiC polytypes. *Phys. Status Solidi A* **162**(1), 39 (1997).
65. S. Sorieul, J.M. Costantini, L. Gosmain, L. Thome, and J.J. Grob: Raman spectroscopy study of heavy-ion-irradiated alpha-SiC. *J. Phys.: Condens. Matter* **18**(22), 5235 (2006).
66. H. Yugami, S. Nakashima, A. Mitsuishi, A. Uemoto, M. Shigeta, K. Furukawa, A. Suzuki, and S. Nakajima: Characterization of the free-carrier concentrations in doped beta-SiC crystals by Raman-scattering. *J. Appl. Phys.* **61**(1), 354 (1987).
67. M.R. Tonks, P.C. Millett, P. Nerikar, S. Du, D. Andersson, C.R. Stanek, D. Gaston, D. Andrs, and R. Williamson: Multiscale development of a fission gas thermal conductivity model: Coupling atomic, meso and continuum level simulations. *J. Nucl. Mater.* **440**(1–3), 193 (2013).
68. C. Valot, M. Bertolus, R. Konings, J. Somers, and S. de Groot: Basic research in support of innovative fuels design for the GEn IV systems: The F-BRIDGE project. *Nucl. Eng. Des.* **241**(9), 3521 (2011).
69. S. Nichenko and D. Staicu: Molecular Dynamics study of the effects of non-stoichiometry and oxygen Frenkel pairs on the thermal conductivity of uranium dioxide. *J. Nucl. Mater.* **433**(1–3), 297 (2013).
70. M.R. Tonks: *Neams Software V&V Plan for the MARMOT Software* (Idaho National Laboratory, Idaho Falls, m 2014).
71. D. Petti, J. Maki, J. Hunn, P. Pappano, C. Barnes, J. Saurwein, S. Nagley, J. Kendall, and R. Hobbins: The DOE advanced gas reactor fuel development and qualification program. *JOM* **62**(9), 62 (2010).
72. D.A. Petti, J. Buongiorno, J.T. Maki, R.R. Hobbins, and G.K. Miller: Key differences in the fabrication, irradiation and high temperature accident testing of US and German TRISO-coated particle fuel, and their implications on fuel performance. *Nucl. Eng. Des.* **222**(2–3), 281 (2003).
73. D.A. Petti, P.A. Demkowicz, J.T. Maki, and R.R. Hobbins: TRISO-coated particle fuel performance. *Compr. Nucl. Mater.* **3**, 151 (2012).
74. K. Verfondern: Triso fuel performance modeling and simulation. *Compr. Nucl. Mater.* **3**, 755 (2012).
75. G.K. Miller, D.A. Petti, J.T. Maki, and D.L. Knudson: Updated solution for stresses and displacements in TRISO-coated fuel particles. *J. Nucl. Mater.* **374**(1–2), 129 (2008).
76. B.P. Collin, D.A. Petti, P.A. Demkowicz, and J.T. Maki: Comparison of fission product release predictions using PARFUME with results from the AGR-1 safety tests. *Nucl. Eng. Des.* **301**, 378 (2016).
77. D. Rochais, G. Le Meur, V. Basini, and G. Domingues: Microscopic thermal characterization of HTR particle layers. *Nucl. Eng. Des.* **238**(11), 3047 (2008).
78. G.K. Miller, D.A. Petti, J.T. Maki, and D.L. Knudson: *PARFUME Theory and Model Basis Report* (Idaho National Laboratory, Idaho Falls, 2009).
79. J.T. White, A.T. Nelson, J.T. Dunwoody, D.D. Byler, D.J. Safarik, and K.J. McClellan: Thermophysical properties of U_3Si_2 to 1773 K. *J. Nucl. Mater.* **464**, 275 (2015).
80. G.J. Butterworth and C.B.A. Forty: A survey of the properties of copper-alloys for use as fusion-reactor materials. *J. Nucl. Mater.* **189**(3), 237 (1992).
81. W. Schilling and H. Ullmaier: *Physics of Radiation Damage in Metals, in Materials Science and Technology* (Wiley, Berlin, 2006).
82. L.L. Snead, T. Nozawa, Y. Katoh, T.S. Byun, S. Kondo, and D.A. Petti: Handbook of SiC properties for fuel performance modeling. *J. Nucl. Mater.* **371**(1–3), 329 (2007).
83. S.J. Zinkle and L.L. Snead: Designing radiation resistance in materials for fusion energy. *Annu. Rev. Mater. Res.* **44**(1), 241 (2014).
84. Y. Katoh, L.L. Snead, C.H. Henager, Jr., T. Nozawa, T. Hinoki, A. Ivekovic, S. Novak, and S.M.G. de Vicente: Current status and recent research achievements in SiC/SiC composites. *J. Nucl. Mater.* **455**(1–3), 387 (2014).
85. Y. Katoh, T. Nozawa, and L.L. Snead: Mechanical properties of thin pyrolitic carbon interphase SiC-matrix composites reinforced with near-stoichiometric SiC fibers. *J. Am. Ceram. Soc.* **88**(11), 3088 (2005).
86. Y. Katoh, K. Ozawa, C. Shih, T. Nozawa, R.J. Shinavski, A. Hasegawa, and L.L. Snead: Continuous SiC fiber, CVI SiC matrix composites for nuclear applications: Properties and irradiation effects. *J. Nucl. Mater.* **448**(1–3), 448 (2014).
87. S. Bragg-Sitton, K. Barrett, I. van Rooyen, D. Hurley, and M. Khafizov: Studying silicon carbide for nuclear fuel cladding. *Nucl. Eng. Int.* **58**(706), 37 (2013).
88. D.H. Hurley, M. Khafizov, and S.L. Shinde: Measurement of the Kapitza resistance across a bicrystal interface. *J. Appl. Phys.* **109**(8), 083504 (2011).